Digest Journal of Nanomaterials and Biostructures Vol. 20, No. 4, October-December 2025, p. 1363-1380

4-Nitroaniline picric acid single crystals: unveiling their complete optoelectronic potential through optical, thermal, and quantum chemical characterization

N. Saranya [a,b], R. Karunathan [a,*], B. Balraj [c], S. Selvaraj [d], M. Gowtham [e]
[a] *Department of Physics, Dr.N.G.P. Arts and Science College, Coimbatore 641048, Tamilnadu, India*
[b] *Department of Physics, Jansons Institute of Technology, Karumathampatti, Coimbatore-641 659, Tamilnadu, India.*
[c] *Department of Physics, Vel Tech Rangarajan Dr. Sagunthala R&D Institute of Science and Technology,Chennai, 600 062,*
[d] *Department of Physics, Saveetha School of Engineering, Saveetha Institute of Medical and Technical Sciences (SIMATS), Thandalam, Chennai, 602105, Tamil Nadu, India.*
[e] *Postgraduate and Research Department of Physics, Nanotechnology Lab, Kongunadu Arts and Science College, Coimbatore, 641029, Tamil Nadu, India*

Single crystals of 4-nitroaniline picric acid (NANP), with dimensions of 5 × 2 × 1 mm³, were synthesized by the solution growth method employing acetone as the solvent. The crystalline quality of the synthesized material was verified by powder X-ray diffraction (XRD) analysis. Optical assessment via UV-Vis spectroscopy established that the crystals show excellent transparency throughout the visible range (400–800 nm), underlining their prospective utility in optoelectronic applications that demand efficient light transmission. Thermal stability investigations conducted through thermogravimetric analysis (TGA) and differential thermal analysis (DTA). Further molecular functional groups and their vibrational characteristics were analysed by FT-IR and Raman spectroscopies. The nonlinear optical properties were explored with the Z-scan technique for screening its capability for nonlinear optical devices. In addition, to furnish a detailed perspective on the electronic structure, including the distribution of frontier molecular orbitals (HOMO-LUMO), thermodynamic characteristics, and the first hyperpolarizability analysis were done utilizing Gaussian 09 and the HF or B3LYP/6-311++G(d,p) basis sets.

(Received July 26, 2025; Accepted October 27, 2025)

Keywords: Nonlinear, Solution growth, FT-Raman, Nitroaniline, Picric acid, DFT

1. Introduction

In recent years, the demand for optically active organic crystals has increased significantly due to their extensive applications in electro-optic modulators, optical storage devices, terahertz wave generation and detection, laser fusion reactions, optical signal processing, color displays, frequency conversion, photonics, laser remote sensing, and medical diagnostics [1]. To cater to the needs of current civilization, the synthesis and characterization of nonlinear optical (NLO) materials with special features and low cost have become increasingly demanding research areas [2]. Several approaches have been proposed to achieve non-centrosymmetric crystal lattices, including meta substitution, introducing chiral centers, vanishing dipole moments, and utilizing non-covalent interactions [3]. One particularly fascinating approach involves proton transfer between two separate organic chromophores one acidic and another basic in various cation-anion combinations to enhance their asymmetric nature [4]. The conjugated π-electron moiety provides a pathway for charge delocalization across the entire length of conjugation under the perturbation of an external electric field, making these systems highly promising for advanced nonlinear optical applications [5].

* Corresponding author: karunathan.phd@gmail.com
https://doi.org/10.15251/DJNB.2025.204.1363

Generally, organic materials demonstrate superior versatility compared to inorganic counterparts, exhibiting large nonlinear optical properties with almost unlimited design possibilities for second harmonic generation (SHG) [6]. These materials possess excellent characteristics including high electronic susceptibility ($\chi(2)$), fast response times, and high resistance to optical damage [7]. Notably, the electronic susceptibility (χe) of organic NLO materials is several orders of magnitude higher than that of inorganic materials, while also offering higher molecular polarizability (β), higher laser damage thresholds, ease of device fabrication and flexibility in molecular design through proper synthetic methods [8].

Among the various organic CT complexes, those involving a strong electron acceptor with aromatic amines have drawn particular attention due to their ability to form crystalline materials with large hyperpolarizabilities, broadband transparency, and appreciable thermal stability [9]. The 4-nitroaniline–picric acid cocrystal is such a material where donor–acceptor interactions induce substantial intermolecular charge transfer a mechanism central to elevated second and third-order nonlinear optical efficiency [10]. So, in this present work 4-nitroaniline–picric acid crystals have been grown using slow evaporation solution growth technique and their physiochemical properties were studied. Also, their quantum chemical properties

2. Methodology

2.1. Crystal growth

High quality single crystals of 4-Nitroaniline picric acid (NANP) were prepared by a slow evaporation solution growth method at room temperature. 4-nitroaniline and picric acid (E-Merck) were measured in a stoichiometric (2:1) molar ratio. To initiate crystal growth, each compound was separately dissolved in ethanol and stirred constantly for 30 minutes. Subsequently, the solutions were combined and stirred for an additional 30 minutes to ensure thorough mixing. The resultant saturated solution was then transferred to a crystallization vessel, covered with a thin plastic sheet to achieve controlled evaporation. The undisturbed vessel was left at room temperature to facilitate slow solvent evaporation. After two weeks, rhombus-shaped crystals with approximate dimensions of 5 x 2 x 1 mm^3 were successfully harvested from the remaining mother liquor. A photograph of a representative crystal is presented in Figure 1.

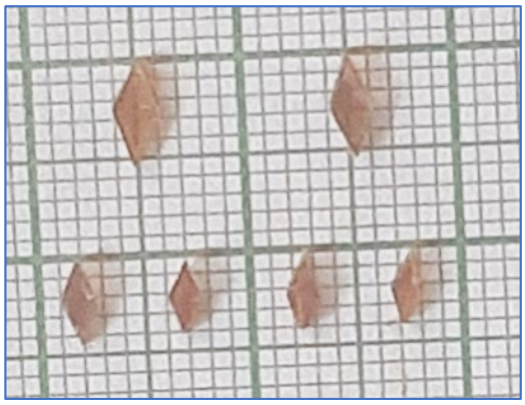

Fig. 1. The grown crystal of the compound 4-nitroaniline picric acid.

2.2. Characterization techniques

To achieve a thorough understanding of the synthesized NANP crystals, an array of advanced characterization methods was systematically employed for the elucidation of their crystal structure, chemical composition, and thermal behavior. Functional moieties within the crystal matrix were identified using Fourier-Transform Infrared (FT-IR) spectroscopy, specifically with a

Shimadzu IR Affinity-1S double-beam instrument. This provided high-resolution spectra (4000–500 cm^{-1}, 0.5 cm^{-1} resolution), enabling unambiguous assignment of characteristic vibrational bands related to distinct functional groups. Additional insight into molecular vibrations was obtained from Raman spectroscopy, performed with a confocal micro-Raman system scanning the 50–4000 cm^{-1} range. This facilitated the precise mapping of vibrational modes complementary to IR selection rules. To assess optical absorption characteristics, a UV-visible study was carried out on an ethanolic solution of the crystals using a PerkinElmer Lambda 365 spectrophotometer within the 200–700 nm region. This identified absorption edges and optical transparency critical for optoelectronic relevance. To investigate thermal robustness, a Hitachi STA7000 for simultaneous thermogravimetric (TGA) and differential thermal analysis (DTA), thereby tracking mass loss and enthalpic transitions as functions of temperature to reveal decomposition pathways and stability windows. Furthermore, Nuclear Magnetic Resonance (NMR) spectroscopy either ^{1}H or ^{13}C was proposed for elucidating molecular architecture at the atomic level by correlating chemical shifts to proton and carbon environments, which can deepen the structural assignment beyond vibrational spectroscopy. This multifaceted approach ensures that structural, spectroscopic, and stability aspects of NANP crystals are thoroughly characterized, laying a robust foundation for both fundamental studies and applications in nonlinear optics.

2.3 Computational details

Simulation was carried out using density functional theory (DFT) of the Gaussian 09W software package [11] to gain profound knowledge on the structural and vibrational characteristics of 4-nitroaniline picric acid (NANP) at molecular level. Two established functionals were used: the Hartree-Fock (HF) method which is a basic method for calculating the electronic structure, and the B3LYP method, a so-called hybrid method which combines the Hartree-Fock exchange with DFT. The two basis sets were used with each functional were the commonly employed 6-31++G basis set, used for general calculations in computational chemistry and the extended basis set 6-311++G(d,p), which utilise diffuse functions to better describe such molecules [12, 13]. These calculations primarily aimed at optimizing the ground state geometry of the NANP molecule and calculating the vibrational frequencies associated with different atomic motions within the molecule. Interestingly, a comparison of these simulated frequencies with experimental FT-IR and Raman frequencies (though not explicitly mentioned here like derived previously) can provide useful validation for the computational model. The present integrated theoretical calculations and experimental characterization give a complete picture of the structure and infrared vibrations of NANP crystals.

3. Results and discussion

3.1. XRD studies

X-ray diffraction (XRD) was conducted to measure the level of crystallinity and elucidate the crystallographic properties of synthesized 4-nitroaniline picric acid (NANP). The principle of XRD relies on the assumption that the emitted X-rays are incident on the crystalline matter in such that their diffraction pattern can be interpreted. This process is mainly controlled by Bragg Law: $n\lambda=2d\sin\theta$, in which λ represents the wavelength of incident X-rays, d- the interplanar spacing, and θ- the Bragg angle [14]. The XRD profile of NANP (see Fig. 2) exhibits several strong and sharp reflections in the 2ɵ range between 10 and 70 d. Such clean peaks are a hallmark of high structural order and strong crystallinity in the sample. The absence of broad and diffused peaks, which are typically characteristic of amorphous phases, further reinforces the crystalline nature of the sample [15]. Such clear Bragg peaks indicate successful crystal growth and provide a solid structural basis for further detailed optical, thermal and theoretical analysis.

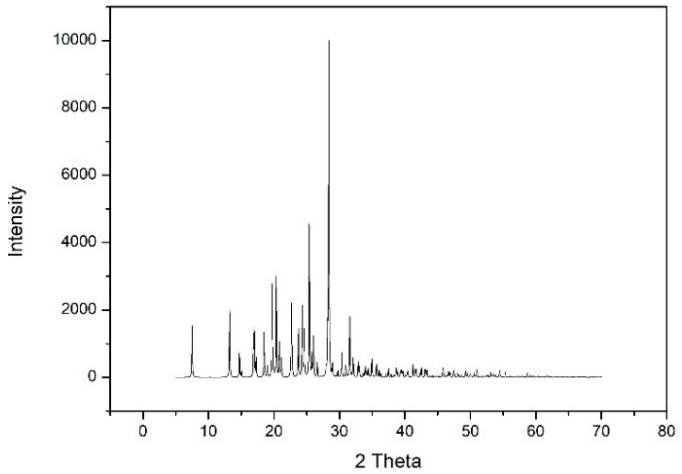

Fig. 2. The XRD spectrum of the compound 4-nitroaniline picric acid.

3.2. FT-IR spectral study

To determine the functional groups, present in synthesized 4-nitroaniline picric acid (NANP) crystals, Fourier-Transform Infrared (FT-IR) spectroscopy was performed (Figure 3). The final FT-IR spectrum acquired displayed clear absorption peaks, identifying different types of molecular vibrations. This indicated that the crystal was able to accommodate specific functional groups. O-H stretching was assigned to a broad absorption of 3479 cm^{-1}, indicating the presence of hydroxyl moieties. Its band at 3358 cm^{-1}, attributed to N-H stretching, is shifted to a lower frequency than normal, which may be attributed to hydrogen bonding in the crystalline phase. The stretching of aromatic C-H was observed at 3109 cm^{-1}. The sharp band at 1587 cm^{-1} was related to N H bending, and the strong band at 1502 cm^{-1} to the asymmetric stretching of the nitro (NO_2) group. The 1444 cm^{-1} and 1394 cm^{-1} absorptions were assigned to aromatic C-C stretching, the downshift of the latter, with respect to literature values, suggests intermolecular effects in the crystal phase. The peak at 1294 cm^{-1} identified the presence of C-N str; 1109 cm^{-1} band indicated the in-plane C-H bending; and the 964 cm^{-1} absorption was evidence of the C-NO_2 stretching. Lastly, the absorption signal at 750 cm^{-1} was assigned to out-of-plane C-H bend [16,17]. Altogether, the existence of such typical vibrational bands and their exact locations confirm that all expected functional groups are incorporated into the NANP crystal structure successfully and consistent with the similar assignments of such organic compounds reported in the literature based on FT-IR spectroscopy.

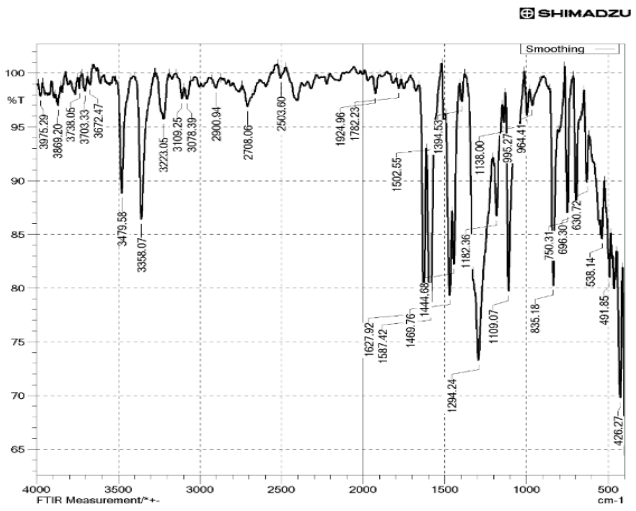

Fig. 3. FT-IR Analysis of 4NANP.

3.3. FT-Raman analysis

Raman spectroscopy was utilized to thoroughly examine the vibrational modes present within the 4-nitroaniline picric acid (NANP) crystals (Figure 4). The resulting spectrum is characterized by distinct bands at 3560, 3363, 3184, 2887, 2782, 1594, 1318, 1287, 1111, and 866 cm^{-1}, many of which demonstrate notable intensity enhancement relative to the reference spectrum. Specifically, the very strong signal at 1594 cm^{-1} is attributed to C-C stretching vibrations, and indicates a high degree of delocalization of the π electrons of the aromatic structure in electron-rich regions. Furthermore, a band appears at 1111 cm^{-1} corresponding to in-plane C-H bending, indicating a significant degree of energy stabilization through C-H bond bending [18]. Moreover, the peaks at 1318 cm^{-1}, 1287 cm^{-1} and 866 cm^{-1} are assigned to symmetric stretching of NO_2 (Nitro), C-N stretching and NO_2 bending vibrations respectively. The presence of N-H stretching is demonstrated by the sharp band at 3363 cm^{-1}, suggesting that molecular interactions or hydrogen bonds play a role in the formation of the crystalline matrix. Additionally, it should be mentioned that the strong rise in the C-C stretching band positions at 1594 cm^{-1} indicates strong intermolecular interactions or lattice thermodynamics, which can be directly linked to NANP's unusual structural arrangement. A thorough comprehension of molecular vibrations and functional group distributions in NANP crystals is attained when these assignments are combined with the FT-IR data. It is well known that this combined spectroscopic approach can be used to clarify the intermolecular dynamics and molecular structure of crystalline organic compounds.

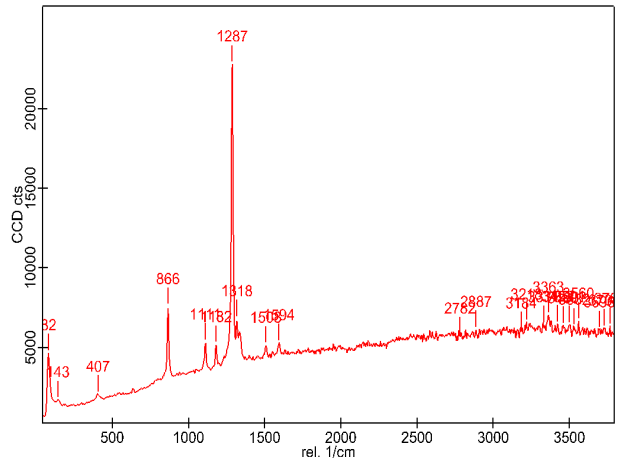

Fig. 4. FT- RAMAN Analysis of 4NANP.

3.4. UV-visible absorption spectrum

The suitability of 4-nitroaniline picric acid (NANP) crystals for light-transmitting optoelectronic applications was evaluated using UV-visible (UV-Vis) absorption spectroscopy. A thin crystal film was analysed using a PerkinElmer Lambda 365 spectrophotometer between 200 and 700 nm (Figure 5). The resulting spectrum revealed a key characteristic, exceptional transparency throughout the visible region (380-700 nm), corresponding to a cut-off wavelength of around 290 nm. This minimal absorption within the visible range suggests a low concentration of chromophores within the NANP crystal lattice. Light absorption in the UV-Vis region is typically governed by electronic transitions such as $\sigma \rightarrow \sigma^*$, $n \rightarrow \sigma^*$, $n \rightarrow \pi^*$, and $\pi \rightarrow \pi^*$ [19]. The observed high transparency across the visible spectrum signifies that NANP crystals efficiently transmit light in this range. This property renders them highly promising candidates for diverse optoelectronic applications that require unobstructed light propagation.

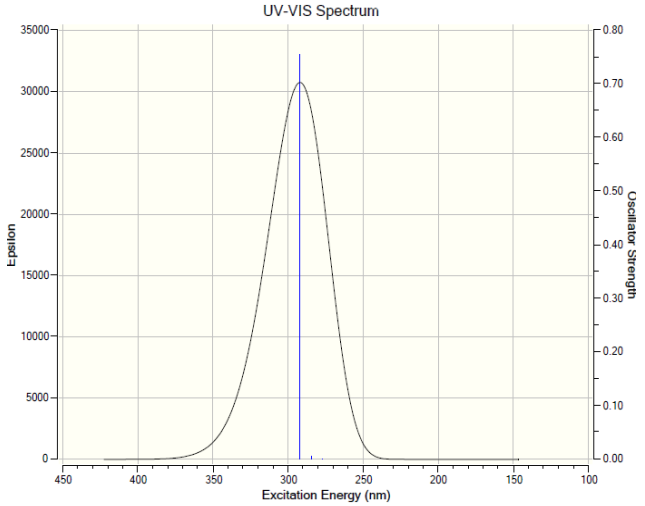

Fig. 5. UV-vis analysis of 4NANP.

3.5. Thermal analysis

Thermogravimetric analysis (TGA) and comparative thermal analysis (DTA) were performed in a nitrogen atmosphere on a Hitachi STA7000 instrument to establish the thermostability of 4-nitroaniline picric acid (NANP) crystals for potential non-linear optical (NLO) applications. A minute sample weighing approximately 13.5 mg was heated to 50 to 750 ºC at the heating rate of 400 ºC /min (see figure 6). Because the TG curve showed only one weight loss, NANP crystals were shown to have strong heat stability. The presence of the residual solvent or impurities in the crystal lattice may be the cause of a tiny peak that was seen below 150 oC [20]. The substantial weight loss in the TG curve most likely corroborated the strong endothermic peak in the DTA curve at about 298 °C, which was the melting temperature of NANP crystals. This high peak also shows that the material has good crystallinity. There were no additional endothermic or exothermic peaks found in any of the thermograms before the melting point, suggesting that no additional phase changes had place before the material entered the melt phase. In conclusion, the combined TGA/DTA results demonstrate that NANP crystals have great thermal stability up to 298 °C, indicating their potential for usage in a variety of NLO applications that call for thermally stable materials.

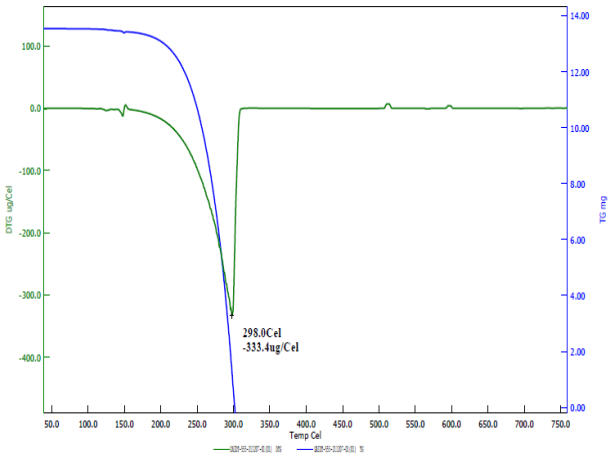

Fig. 6. TG/DTA analysis of 4NANP.

3.6. Z-Scan studies

The well-recognized and established Z-scan technique was adopted to quantitatively evaluate the nonlinear optical (NLO) response of the prepared 4-nitroaniline picric acid (NANP) crystals. The technique is widely used to parameterize the nonlinear refractive index (n_2) and the nonlinear absorption coefficient (β), which play crucial roles in characterizing the third-order nonlinear optical susceptibility ($\chi^{(3)}$) of advanced materials [21]. A NANP crystal sample was prepared by polishing to a size of 4 × 4 × 1 mm³ along the z-axis with respect to the focal point of a continuous wave (CW) He-Ne laser beam (see Table 4 and Table 5 for additional details about the beam). A spatially resolved measurement of the light-matter interaction was thus possible. With the open-aperture setting, the inclusion of an aperture in the detector's path permitted straightforward evaluation of the intensity-dependent absorption and the associated nonlinear absorption coefficient. Alternatively, instead of the open-aperture arrangement, a limited far-field aperture (closed-aperture) was used. This setup was sensitive to the phase shift caused by the optical nonlinearity, enabling precise measurement of the nonlinear refractive index n_2. The fundamental idea behind this measurement is that the normalized transmittance T(z) will exhibit characteristic variations as the sample passes through the focused laser beam. These variations can be rigorously analyzed to reveal n_2 and β. Figure 7 shows the normalized intensity transmittance curves measured under both open- and closed-aperture conditions. The following data analysis, presented in the detailed sections, allows the accurate determination of NLO parameters essential for assessing NANP's suitability in photonic and optoelectronic applications. The flexibility and sensitivity of the Z-scan technique have led to its widespread application as a viable tool for measuring third-order NLO materials, a method highly documented in recent literature [22].

In the Z-scan technique, the differential transmittance between peak and valley positions (ΔT_{p-v}) quantifies the nonlinear phase modulation imparted by the sample, described by:

$$\Delta T_{p-v=0.406\,(1-S)^{0.25}\,|\Delta\phi|} \tag{1}$$

where $\Delta\phi$ signifies the on-axis phase shift at the beam waist, and S (the fractional transmission through the aperture) is evaluated as:

$$S = 1 - exp[\frac{-2r_a^2}{\omega_a^2}] \tag{2}$$

with r_a representing an aperture radius and ω_a the incident beam radius at the aperture. The extraction of the material's nonlinear refractive index, n2n2, follows the relation:

$$n_2 = \frac{\Delta\phi}{kI_0L_{eff}} \tag{3}$$

wherein k=2π/λ, λ is the laser wavelength, I_0 the focal-point intensity, and L_{eff} the effective interaction length, given by:

$$L_{eff} = \frac{1 - e^{(-\alpha L)}}{\alpha} \tag{4}$$

where α is the linear absorption and L the thickness. Furthermore, the nonlinear optical absorption coefficient (β) is extracted from open-aperture Z-scan data via:

$$\beta = \frac{2\sqrt{2}\,\Delta T}{I_0L_{eff}} \tag{5}$$

Analysis of the Z-scan measurements for 4-nitroaniline picric acid (NANP) crystals yields a positive nonlinear refractive index ($n2$) of 1.1075 x 10^{-8} cm²/W and a nonlinear absorption coefficient (β) of 4.233 x 10^{-5} cm/W. The positive value of $n2$ is indicative of a self-focusing

phenomenon, wherein an intensity-dependent refractive index leads to the concentration of light within the medium an effect well-documented in nonlinear optical crystals and essential for applications such as optical switching and beam shaping [1, 14]. The observed asymmetry in the Z-scan traces, particularly under continuous-wave (CW) He-Ne laser excitation, points towards a dominant thermo-optic mechanism governing the nonlinear behavior. In this process, absorbed optical energy is converted to heat, producing a temperature gradient and, consequently, a local modification of the refractive index [10, 23, 24]. Such thermally induced refractive nonlinearities are especially prominent under conditions of significant linear absorption and moderate power densities, where thermal lensing can dominate the measured $n2$ [15][5]. The corresponding third-order nonlinear susceptibility ($\chi^{(3)}$) for the NANP crystal crucial for quantifying the overall third-order response is comprehensively summarized in Table 1.

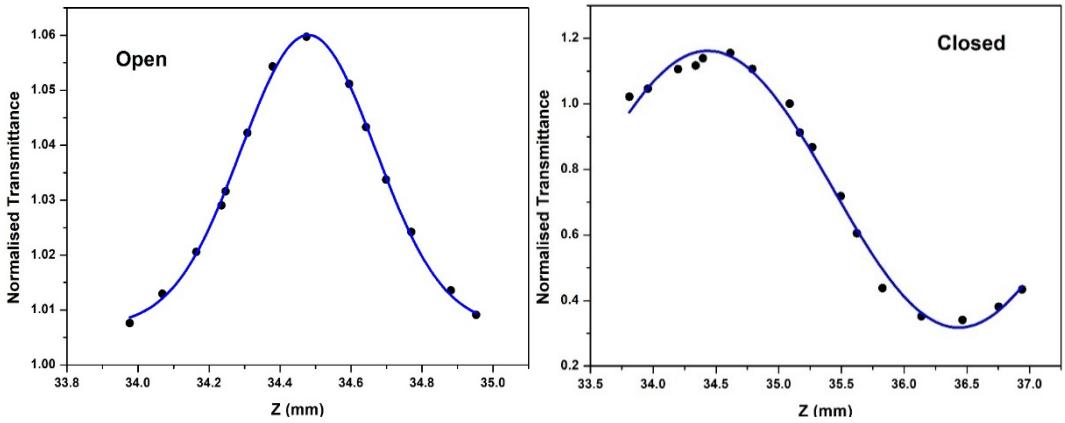

Fig. 7. Z scan curve for (a) open and (b) closed aperture mode.

3.7. Optimized parameters

Figure 8 displays the optimized geometry of a single NANP molecule, including the atomic symbols and numbering scheme used for subsequent computational analysis. The computed structural parameters for NANP, as detailed in Table 1, are compared with experimental single-crystal X-ray diffraction (SXRD) data. Notably, the computed O32···H15 and O33···H29 bond distances are 1.822 Å and 1.759 Å, respectively—considerably shorter than the sum of the van der Waals radii for O···H (2.72 Å), thereby demonstrating strong intramolecular hydrogen bonding interactions. These findings confirm the existence of intramolecular N7–H15···O32 and O28–H29···O33 hydrogen bonds in the NANP molecule. Furthermore, the presence of N–H···O and O–H···O interactions leads to subtle elongation of the N7–H15 (1.033 Å), O28–H29 (0.992 Å), N26–O32 (1.274 Å), and N26–O33 (1.287 Å) bonds when compared to typical values. This also results in a slight decrease of the H8–N7–H15 bond angle (116.60°). These geometric shifts are characteristic signatures of hydrogen-bond formation in organic systems, where such close contact distances and bond angle modifications are supported by SXRD and neutron diffraction studies conducted on other hydrogen-bonded small molecules and biomacromolecules. The dihedral angles of C6-N9-H29-O28 and O10-N9-H29-O28 are calculated to be 164.20º and 164.66º, respectively. Upon substitution of the O-H group, the bond distance of C22-C23 (1.433 Å), C23-C24 (1.417 Å) are slightly elongate compare to other C-C bond distance in the phenyl ring. Additionally, the bond angles of C2-C4-C6 (118.81º), C6-C13-C11 (118.95º) are decreased and C4-C6-C13 (123.02º) is increased. Due to the interaction between -OH and NO_2 group, the bond angles of C20-C22-N26 (117.89º), C17-C24-N27 (117.04º) are shorten while C23-C22-N26 (120.34º), C23-C24-N27 (121.07º) are lengthen compared to other C-C-N bond angles. The dihedral angles of the N7-C1-C2-C4 (-179.96º), C11-C1-C2-C4 (0.03º), C2-C1-C11-C13 (-0.02º), C7-C1-C11-C13 (179.97º), C1-C2-C4-C6 (-0.01º), C2-C4-C6-N9 (179.98º), C2-C4-C6-C13 (-0.02º), C4-C6-N9-O10 (0.19º), C4-C6-N9-O16 (-179.80º), C13-C6-N9-O10 (-179.81º) C13-C6-N9-O16 (0.19º), C4-C6-C13-C11 (0.03º), N9-C6-C13-C11 (-179.97º), C1-C11-C13-C6 (-0.01º),

C24-C17-C19-C20 (-1.08º), C24-C17-C19-N25 (179.11º), C17-C19-C20-C22 (-0.28º), N25-C19-C20-C22 (179.54º), C17-C19-N25-O30 (-0.38º), C17-C19-N25-O31 (179.64º), C20-C19-N25-O30 (179.80º), C20-C19-N25-O31 (-0.18º), C19-C20-C22-C23 (0.72º), C19-C20-C22-N26 (-179.03º), C20-C22-C23-C24 (0.18º), N26-C22-C23-C24 (179.92º) and C23-C22-N26-O32 (179.17º) bonds are shown to exhibit co-planar orientation as computed by DFT calculation.

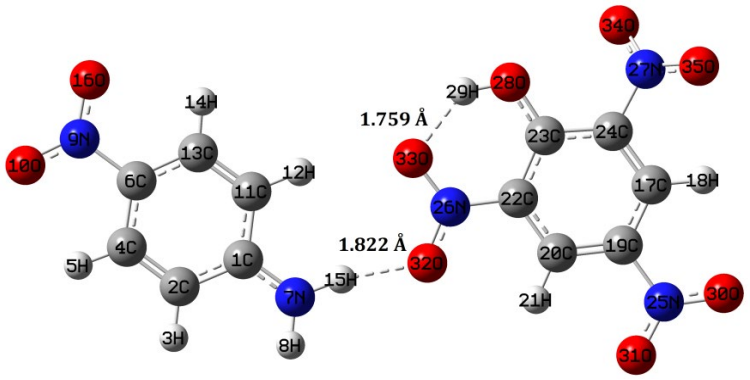

Fig. 8. Optimized structure of NANP.

Table 1. Optimized parameters of NANP.

Bond lengths	B3LYP (Å)	XRD (Å)	Bond Angles	B3LYP (°)	XRD (°)	Dihedral Angles	B3LYP (°)	XRD (°)
C1-C2	1.441	1.402	C2-C1-N7	120.46	120.80	N7-C1-C2-H3	0.02	-0.37
C1- N7	1.339	1.355	C2-C1-C11	120.09	118.39	N7-C1-C2-C4	-179.96	179.68
C1-C11	1.442	1.402	N7-C1-C11	119.45	120.80	C11-C1-C2-H3	-179.99	179.63
C2-H3	1.085	0.930	C1-C2-H3	119.71	119.66	C11-C1-C2-C4	0.03	-0.32
C2-C4	1.378	1.366	C1-C2-C4	119.66	120.67	C2-C1-N7-H8	-0.03	-0.08
C4-H5	1.082	0.930	H3-C2-C4	120.64	119.67	C2-C1-N7-H15	179.90	179.92
C4-C6	1.411	1.381	C2-C4-H5	121.97	120.14	C11-C1-N7-H8	179.98	179.92
C6-N9	1.476	1.458	C2-C4-C6	118.81	119.69	C11-C1-N7-H15	-0.10	-0.08
C6-C13	1.409	1.381	H5-C4-C6	119.23	120.18	C2-C1-C11-H12	179.99	179.63
N7-H8	1.016	0.860	C4-C6-N9	118.44	119.55	C2-C1-C11-C13	-0.02	-0.32
N7-H15	1.033	0.860	C4-C6-C13	123.02	120.90	N7-C1-C11-H12	-0.02	-0.37
N9-O10	1.260	1.217	N9-C6-C13	118.54	119.55	C7-C1-C11-C13	179.97	179.68
N9-O16	1.259	1.217	C1-N7-H8	120.95	120.00	C1-C2-C4-H5	179.99	-179.35
C11-H12	1.085	0.930	C1-N7-H15	122.45	120.00	C1-C2-C4-C6	-0.01	0.64
C11-C13	1.379	1.366	H8-N7-H15	116.60	120.00	H3-C2-C4-H5	0.00	0.69
C13-H14	1.082	0.930	C6-N9-O10	117.07	118.86	H3-C2-C4-C6	-180.00	-179.32
C17-H18	1.083	0.931	C6-N9-O16	117.10	118.86	C2-C4-C6-N9	179.98	179.68
C17-C19	1.403	1.404	O10-N9-O16	125.82	122.29	C2-C4-C6-C13	-0.02	-0.32
C17-C24	1.383	1.408	C1-C11-H12	119.18	119.66	H5-C4-C6-N9	-0.03	-0.33
C19-C20	1.378	1.363	C1-C11-C13	119.47	120.67	H5-C4-C6-C13	179.98	179.67
C19-N25	1.471	1.476	H12-C11-C13	121.35	119.67	C4-C6-N9-O10	0.19	4.82
C20-H21	1.082	0.930	C6-C13-C11	118.95	119.69	C4-C6-N9-O16	-179.80	-175.18
C20-C22	1.406	1.370	C6-C13-H14	119.19	120.17	C13-C6-N9-O10	-179.81	-175.18
C22-C23	1.433	1.377	C11-C13-H14	121.87	120.14	C13-C6-N9-O16	0.19	4.82
C22-N26	1.423	1.463	H18-C17-C19	120.59	122.31	C4-C6-C13-C11	0.03	-0.32
C23-C24	1.417	1.382	H18-C17-C24	120.08	122.33	C4-C6-C13-H14	-179.99	179.67
C23-O28	1.338	1.382	C19-C17-C24	119.33	115.36	N9-C6-C13-C11	-179.97	179.68
C24-N27	1.475	1.455	C17-C19-C20	121.85	122.49	N9-C6-C13-H14	0.02	-0.33
N25-O30	1.258	1.178	C17-C19-N25	119.31	120.81	C6-N9-H29-O28	164.20	-174.03
N25-O31	1.261	1.265	C20-C19-N25	118.84	116.69	O10-N9-H29-O28	164.66	-159.03
N26-O32	1.274	1.216	C19-C20-H21	120.52	120.25	C1-C11-C13-C6	-0.01	0.64

Bond lengths	B3LYP (Å)	XRD (Å)	Bond Angles	B3LYP (°)	XRD (°)	Dihedral Angles	B3LYP (°)	XRD (°)
N26-O33	1.287	1.255	C19-C20-C22	118.56	119.45	C1-C11-C13-H14	-180.00	-179.36
N27-O34	1.255	1.210	H21-C20-C22	120.92	120.30	H12-C11-C13-C6	179.99	-179.32
N27-O35	1.262	1.229	C20-C22-C23	121.77	121.88	H12-C11-C13-H14	0.00	0.69
O28-H29	0.992	0.820	C20-C22-N26	117.89	118.50	H18-C17-C19-C20	178.69	-178.61
H29-O33	1.759	1.604	C23-C22-N26	120.34	119.62	H18-C17-C19-N25	-1.13	1.90
			C22-C23-C24	116.57	117.64	C24-C17-C19-C20	-1.08	1.33
			C22-C23-O28	124.18	114.44	C24-C17-C19-N25	179.11	-178.16
			C24-C23-O28	119.23	127.65	H18-C17-C24-C23	-177.73	178.61
			C17-C24-C23	121.89	123.16	H18-C17-C24-N27	2.04	-2.11
			C17-C24-N27	117.04	119.39	C19-C17-C24-C23	2.03	-1.64
			C23-C24-N27	121.07	117.44	C19-C17-C24-N27	-178.19	177.96
			C19-N25-O30	117.25	125.67	C17-C19-C20-H21	-179.86	179.48
			C19-N25-O31	117.19	116.56	C17-C19-C20-C22	-0.28	-0.50
			O30-N25-O31	125.56	116.87	N25-C19-C20-H21	-0.05	-1.01
			C22-N26-O32	119.41	116.73	N25-C19-C20-C22	179.54	179.01
			C22-N26-O33	119.84	121.32	C17-C19-N25-O30	-0.38	-7.48
			O32-N26-O33	120.75	121.93	C17-C19-N25-O31	179.64	161.33
			C24-N27-O34	118.09	118.48	C20-C19-N25-O30	179.80	173.00
			C24-N27-O35	116.00	119.13	C20-C19-N25-O31	-0.18	-18.19
			O34-N27-O35	125.87	122.38	C19-C20-C22-C23	0.72	-0.14
			C23-O28-H29	111.79	109.52	C19-C20-C22-N26	-179.03	-179.55
						H21-C20-C22-C23	-179.70	179.88
						H21-C20-C22-N26	0.55	0.48
						C20-C22-C23-C24	0.18	-0.14
						C20-C22-C23-O28	-177.97	174.31
						N26-C22-C23-C24	179.92	-179.26
						N26-C22-C23-O28	1.78	-6.29
						C20-C22-N26-O32	-1.07	16.22
						C20-C22-N26-O33	178.96	-165.09
						C23-C22-N26-O32	179.17	-163.20
						C23-C22-N26-O33	-0.80	15.49
						C22-C23-C24-C17	-1.57	-178.51
						C22-C23-C24-N27	178.67	1.09
						O28-C23-C24-C17	176.67	-172.53
						O28-C23-C24-N27	-3.10	7.87
						C22-C23-O28-H29	-1.18	0.01
						C24-C23-O28-H29	-179.28	173.80
						C17-C24-N27-O34	145.85	-178.11
						C17-C24-N27-O35	-32.09	1.20
						C23-C24-N27-O34	-34.37	1.51
						C23-C24-N27-O35	147.68	-179.19
						C22-N26-O33-H14	178.74	-159.09
						O32-N26-O33-H14	-1.24	11.53

3.8. NBO analysis

Natural Bond Orbital (NBO) analysis at the DFT/B3LYP/6-311++G(d,p) theoretical level was used to gain insight into the electronic structure and intramolecular interactions of the 4-nitroaniline picric acid (NANP) molecule. In this analysis method, the electron density is split into natural localized orbitals, allowing electron delocalization and stabilization can be studied in detail, including quantification of the donor-acceptor interaction and second-order perturbation stabilization energies [25]. The findings indicate that lone pairs (nO) on the oxygen atoms engage in hyper conjugative interactions with the nitro groups' π^* (N-O) antibonding orbitals providing exceptional stabilization effects up to 385 kJ/mol. These lone pairs are significatively engaged in negative hyperconjugation interactions with the molecule, a key factor in its electronic stability.

Moreover, additional electron density transfers from nO to the π* orbitals of the N–H and O–H bonds exist, which indicates the occurrence of intramolecular hydrogen bonding. This stabilization includes interactions which lead to stabilization energies of 10 to 36 kJ/mol, ranges consistent with carefully investigated NBO-based analyses of hydrogen-bonded molecular systems. The analysis also reveals a major π-conjugation within the aromatic core, represented by interactions between π(C–C) and π*(C–C) orbitals with stabilization energies up to 72 kJ/mol. Furthermore, there is additional intramolecular charge transfer whereby lone pairs on nitrogen or carbon are donated into π*(C–C) orbitals (up to 121 kJ/mol). The complete calculated stabilization energies of these processes, derived from the second-order perturbation analysis, have been collected in Table 2.

Table 2. Second-order perturbation theory analysis of Fock matrix in NBO basis including the stabilization energies of NANP.

Donor(i)	**ED(i)**	**Acceptor(j)**	**ED(*j*)**	**E(2)[a]**	**E(*j*)-E(*i*)[b]**	**F(i,j)c**
	(e)		**(e)**	**(kJ/mol)**	**(a.u)**	**(a.u)**
within unit 1						
π(C1-C2)	0.819	π*(C4-C6)	0.199	72.43	0.28	0.09
π(C1-C2)	0.819	π*(C11-C13)	0.135	19.54	0.30	0.05
π(C4-C6)	0.832	π*(C1-C2)	0.221	24.39	0.25	0.05
π(C4-C6)	0.832	π*(N9-O10)	0.329	56.90	0.16	0.06
π(C4-C6)	0.832	π*(C11-C13)	0.135	61.04	0.30	0.08
π(N9-O10)	0.993	π*(N9-O10)	0.329	19.41	0.28	0.06
π(C11-C13)	0.850	π*(C1-C2)	0.221	60.63	0.25	0.08
π(C11-C13)	0.850	π*(C4-C6)	0.199	22.47	0.27	0.05
n1N7	0.903	π*(C1-C2)	0.221	92.59	0.30	0.11
n2O10	0.950	σ*(C6-N9)	0.054	26.74	0.53	0.07
n2O10	0.950	σ*(N9-O16)	0.329	38.07	0.63	0.10
n2O16	0.950	σ*(C6-N9)	0.054	26.82	0.53	0.07
n2O16	0.950	σ*(N9-O10)	0.329	38.16	0.63	0.10
n3O16	0.713	π*(N9-O10)	0.329	385.26	0.11	0.13
unit 2 to unit 1						
n1O32	0.984	σ*(N7-H15)	0.026	14.10	1.23	0.08
n2O32	0.944	σ*(N7-H15)	0.026	32.76	0.77	0.10
within unit 2						
σ(C17-H18)	0.986	σ*(C23-C24)	0.016	10.84	1.03	0.07
π(C17-C24)	0.830	π*(C19-C20)	0.142	29.12	0.29	0.06
π(C17-C24)	0.830	π*(N27-O34)	0.309	40.58	0.18	0.06
π(C19-C20)	0.835	π*(C17-C24)	0.133	50.75	0.29	0.08
π(C19-C20)	0.835	π*(N25-O30)	0.321	52.13	0.16	0.06
π(N25-O30)	0.991	π*(C19-C20)	0.142	11.42	0.42	0.05
π(N25-O30)	0.991	π*(N25-O30)	0.321	17.87	0.29	0.05
π(N26-O32)	0.994	π*(N26-O32)	0.365	20.84	0.27	0.06
π(N27-O34)	0.991	π*(N27-O34)	0.309	15.44	0.32	0.05
σ(O28-H29)	0.994	σ*(C23-C24)	0.016	10.42	1.28	0.07
n1C22	0.449	π*(C19-C20)	0.142	121.21	0.18	0.11
n1O28	0.986	σ*(C22-C23)	0.019	18.20	1.02	0.08
n2O30	0.950	σ*(C19-N25)	0.052	24.98	0.54	0.07
n2O30	0.950	σ*(N25-O31)	0.028	38.99	0.63	0.10
n2O31	0.951	σ*(C19-N25)	0.052	24.64	0.54	0.07
n2O31	0.951	σ*(N25-O30)	0.028	38.20	0.63	0.10
n3O31	0.711	π*(N25-O30)	0.321	370.95	0.11	0.13
n2O32	0.944	σ*(C22-N26)	0.034	24.56	0.66	0.08
n2O32	0.944	σ*(N26-O33)	0.029	26.19	0.62	0.08
n1O33	0.985	σ*(C22-N26)	0.034	11.38	1.13	0.07
n1O33	0.985	σ*(O28-H29)	0.025	10.84	1.21	0.07
n2O33	0.946	σ*(N26-O32)	0.026	36.19	0.66	0.10

n2O33	0.946	σ*(O28-H29)	0.025	36.36	0.76	0.10
n3O33	0.763	π*(N26-O32)	0.365	300.16	0.11	0.12
n2O34	0.949	σ*(C24-N27)	0.052	28.24	0.53	0.08
n2O34	0.949	σ*(N27-O35)	0.034	38.74	0.62	0.10
n2O35	0.949	σ*(C24-N27)	0.052	26.23	0.53	0.07
n2O35	0.949	σ*(N27-O34)	0.034	36.57	0.62	0.09
n3O35	0.705	π*(N27-O34)	0.309	334.64	0.13	0.13

Together, this NBO study reveals a sophisticated interplay of hyperconjugation, hydrogen bonding, conjugation, and charge-transfer effects, which underlie the stability of the NANP molecule and enhance its stability.

3.9. Frontier molecular orbital analysis

Frontier Molecular Orbital (FMO) analysis of the chemical reactivity and electronic characteristics of the 4-nitroaniline picric acid (NANP) molecule was investigated at various levels of DFT/B3LYP/6-311++G(d,p). The FMOs, especially the HOMO and LUMO, are key to a molecule's chemical stability, reactivity, and optoelectronic responsiveness [26, 27]. The spatial distribution of these orbitals, as shown in Figure 9, quantifies that the HOMO is mostly localized over the nitro groups (atoms O34, O35, O28, and O31) and parts of the aromatic ring, whereas, the LUMO is largely localized over amino (-NH22) group as well as the stand-alone aromatic fragments. A computed HOMO-LUMO energy gap of 3.255 eV was found, which is relatively narrow and indicative of an efficient intramolecular charge transfer pathway. Such a small energy difference, potentially influenced by n–π* interactions and π-conjugation, augments the likelihood of strong NLO responses and facilitates electronic transitions upon photoexcitation [28]. This trend is consistent with observations in analogous π-conjugated systems, where reduced gap values are related to enhanced charge delocalization, polarizability, and nonlinear optical susceptibility. These descriptors collectively characterize the molecule's propensity for electron exchange and its overall chemical stability, comparable to their use in contemporary computational studies of reactive organic and π-conjugated materials.

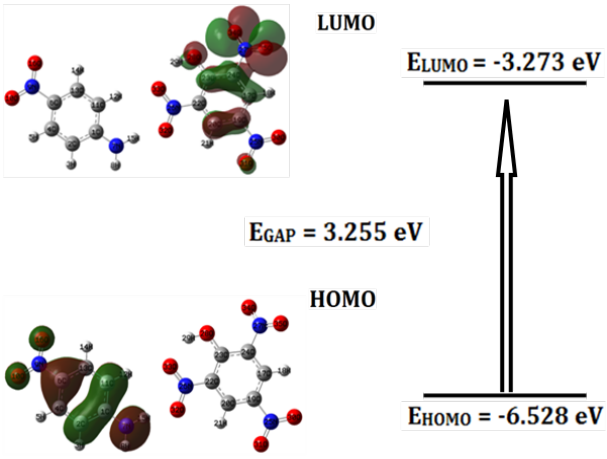

Fig. 9. Frontier molecular orbitals of NANP.

3.10. MEP analysis

To achieve a nuanced understanding of the reactive landscape and intermolecular interaction potential of the 4-nitroaniline picric acid (NANP) molecule, the molecular electrostatic potential (MEP) surface was computed. The MEP provides a three-dimensional visualization of electron density variations across the molecular framework, facilitating the prediction of electrophilic and nucleophilic attack sites [29]. In the color-coded MEP map shown in Figure 10, red delineates electron-rich (highly negative potential) zones, whereas blue marks electron-

deficient (positive potential) regions. For NANP, the red regions are principally situated near the nitro (NO_2) and phenolic (O–H) groups, earmarking these as likely nucleophilic centers capable of interacting with electrophilic species. Conversely, the blue-shaded zones, predominantly associated with the amino (NH_2) group's hydrogen atoms, denote loci that are favorable for nucleophilic attack, corresponding to regions of lower electron density. The observed electrostatic features stem from local electron distribution, where electron-withdrawing nitro and phenol groups accumulate charge, partially shielding the positive nuclear centers in the NH_2 group. This mapping offers a predictive guide to potential chemical reactivity, as validated in recent computational work where MEP surfaces unveiled analogous reactivity trends and interaction propensities in aromatic heterocycles and other bioactive molecules [30]. Therefore, MEP analysis emerges as a critical tool for rationalizing and anticipating the molecular behavior of NANP in diverse chemical environments.

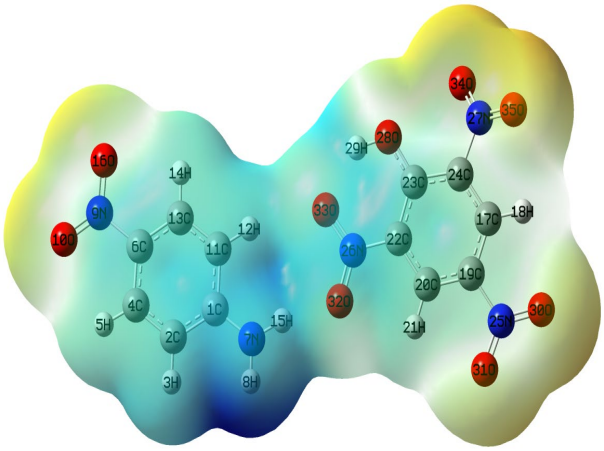

Fig. 10. Molecular electrostatic potential map of NANP.

3.11. Natural population analysis (NPA)

To gain a comprehensive understanding of the intramolecular charge distribution in 4-nitroaniline picric acid (NANP), natural population analysis (NPA) was performed. NPA quantitatively assigns net atomic charges by partitioning electron density, thereby enabling the identification of electron-rich and electron-deficient atomic centers across the molecule [11]. The resulting charge map, shown in Figure 11, reveals the profound impact of hydrogen bonding and atomic electronegativity on charge localization. Specifically, the negative charges observed for hydrogen atoms H8 and H15, which are bonded to the nitrogen atom N7 of the amino group (−0.502e), can be attributed to strong N–H···O hydrogen bonding with the nearby electronegative oxygen atoms an effect consistent with the observed electronic signatures in aromatic systems exhibiting robust intra- or intermolecular hydrogen bonds. Substantial negative charge on O28 (phenolic group) and N7 further establishes these as electron-rich domains, poised to serve as hydrogen bond acceptors or donors in intermolecular interactions. In contrast, the positive charge allocation to selected hydrogen and carbon atoms highlights their role as potential reactive sites for nucleophilic attack, while the persistently negative charges on oxygen atoms in the nitro substituents underscore their electron-withdrawing propensity.

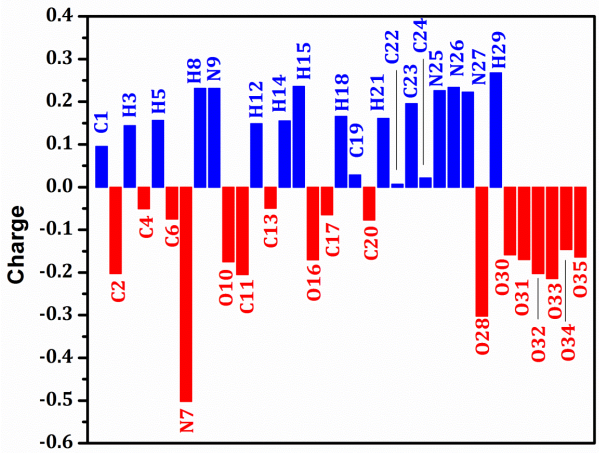

Fig. 11. Natural atomic charge of NANP.

This detailed charge distribution, shaped by hydrogen bonding motifs and the underlying electronegativity gradient, aligns with theoretical findings in structurally analogous molecules, supporting the predictive power of NPA in mapping chemically significant charge polarization [31]. Thus, NPA analysis provides crucial insights into how intra- and intermolecular interactions modulate the electronic structure and reactivity landscape of NANP.

3.12. Thermodynamic properties

The thermodynamic characteristics of the 4-nitroaniline picric acid (NANP) molecule were systematically studied via quantum chemical computations, employing both density functional theory (DFT) and Hartree–Fock (HF) frameworks in conjunction with diverse basis sets. These methodologies enabled the determination of fundamental thermodynamic quantities, including zero-point vibrational energy (ZPVE), thermal energy, specific heat capacity at constant volume (C_v), and entropy (S), the numerical results for which are detailed in Table 3. ZPVE, reflective of the quantum mechanical vibrational motion persisting at absolute zero, displayed discernible dependence on computational method and basis set selection, echoing trends observed in prior vibrational analyses where differences in electron correlation treatment systematically alter vibrational energies. Notably, ZPVE values computed via HF consistently exceeded those from DFT approaches, a pattern that can be attributed to the more limited treatment of electron correlation in HF theory. The computed dipole moment, serving as a measure of molecular polarity and internal charge separation, also varied in response to both the level of theory and the basis set employed—a well-recognized phenomenon in theoretical studies where increasing basis set flexibility and electron correlation generally yield more accurate predictions of molecular electric properties. In addition, the dependence of heat capacity and entropy on temperature was explored through theoretical calculations spanning 100–600 K.

Table 3. The calculated thermodynamic parameter of 4-nitroaniline picric acid.

Thermodynamic parameters	**HF**		**B3LYP**	
	6-31++G(d,p)	**6-311++G(d,p)**	**6-31++G(d,p)**	**6-311++G(d,p)**
Zero-point energy (Kcal/Mol)	157.07	155.74	145.09	143.64
Rotational constant	0.05081	0.04824	0.04548	0.04568
Rotational temperature	0.00244	0.00232	0.00218	0.00219
Energy (E) (Kcal/Mol)				
Translational	0.89	0.89	0.89	0.89
Rotational	0.89	0.89	0.89	0.89
Vibrational	169.10	167.99	157.85	156.61
Total	170.87	169.77	159.63	158.39
Specific heat (C_v)(Kcal/Mol)				
Translational	2.98	2.98	2.98	2.98
Rotational	2.98	2.98	2.98	2.98
Vibrational	72.35	73.51	77.75	78.89
Total	78.31	79.47	83.71	84.86
Entropy (S) (Kcal/Mol)				
Translational	43.59	43.59	43.59	43.59
Rotational	36.83	36.89	36.96	36.96
Vibrational	95.20	98.67	96.07	98.55
Total	175.62	179.16	176.63	179.10
Dipole moment	11.37	11.28	11.74	11.72

As anticipated from statistical thermodynamics, both C_v and S increased monotonically with temperature, a manifestation of progressive activation of vibrational modes and increased molecular disorder at higher thermal energies. Such temperature dependencies are in qualitative agreement with analogous studies of organic molecules and solid-state systems employing DFT-based lattice dynamics or vibrational partition function approaches [32]. In sum, these results affirm the sensitivity of computed thermodynamic properties to the choice of quantum chemical method, underscore the importance of basis set selection, and demonstrate the predictive power of first-principles calculations in capturing the thermodynamic behavior of complex organic molecules.

3.12. Mulliken charge analysis

To supplement the earlier natural population analysis (NPA), Mulliken charge analysis was carried out to offer an alternative quantitative perspective on the electronic charge distribution within the 4-nitroaniline picric acid (NANP) molecule. The detailed Mulliken charges are listed in Table 4 and visualized in Figure 12, revealing how the distribution of atomic charges affects critical molecular properties such as dipole moment, polarizability, and electronic structure. It must be emphasized that Mulliken charges are significantly influenced by the computational methodology both the quantum mechanical approach (Hartree–Fock or DFT) and the chosen basis set due to fundamental differences in the way electron density is partitioned among atomic centers and the degree of electron polarization captured by each method [1, 2]. For instance, the results consistently illustrate a reduction in calculated charges on the N2O3O4 moiety and the NH2 group, irrespective of the method, as well as a persistent positive charge on the C26 atom bound to H35. This aligns with well-established trends: carbon atoms typically function as electron donors (thus acquiring negative Mulliken charges), while hydrogen atoms, acting as electron acceptors, assume positive charges. Notably, the B3LYP function generally predicts greater absolute charge magnitudes than HF; this reflects the inherent sensitivity of Mulliken analysis to the incorporation of electron correlation and basis set expansion. Thus, while Mulliken analysis provides valuable comparative insights, its methodological sensitivity necessitates cautious interpretation and, ideally, comparison with alternative population schemes.

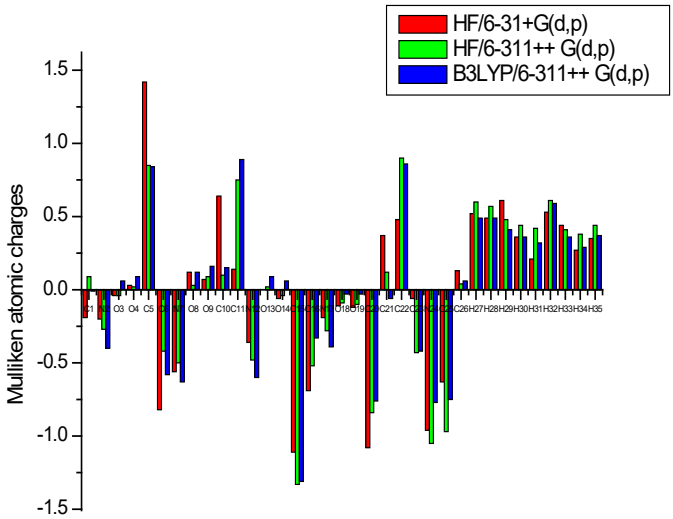

Fig. 12. Mulliken's Atomic charges between theoretical (HF and DFT) approaches.

Table 6. Mullikan atomic charges of 4-nitroaniline picric acid in eV.

Atoms	HF/6-31++G	HF/6-311++G	B3LYP/6-31++G	B3LYP/6-311++G
C1	-0.19	0.09	-0.23	-0.01
N2	-0.20	-0.27	0.97	-0.40
O3	-0.04	-0.04	-0.54	0.06
O4	0.03	0.02	-0.52	0.09
C5	1.42	0.85	0.22	0.84
C6	-0.82	-0.42	-0.38	-0.58
N7	-0.56	-0.50	0.99	-0.63
O8	0.12	0.03	-0.51	0.12
O9	0.07	0.09	-0.51	0.16
C10	0.64	0.10	0.25	0.15
C11	0.14	0.75	-0.44	0.89
N12	-0.36	-0.48	1.15	-0.60
O13	0.00	0.02	-0.55	0.09
O14	-0.06	-0.04	-0.63	0.06
C15	-1.11	-1.33	0.73	-1.31
O16	-0.69	-0.52	-0.80	-0.33
N17	-0.19	-0.28	1.52	-0.39
O18	-0.11	-0.09	-0.72	-0.03
O19	-0.12	-0.10	-0.75	-0.03
C20	-1.08	-0.84	-0.63	-0.76
C21	0.37	0.12	0.26	-0.06
C22	0.48	0.90	-0.33	0.86
C23	-0.06	-0.43	0.91	-0.42
N24	-0.96	-1.05	-1.03	-0.77
C25	-0.63	-0.97	-0.34	-0.75
C26	0.13	0.04	0.26	0.06
H27	0.52	0.60	0.17	0.49
H28	0.49	0.57	0.18	0.49
H29	0.61	0.48	0.47	0.41
H30	0.36	0.44	0.10	0.36
H31	0.21	0.42	0.04	0.32
H32	0.53	0.61	0.31	0.59
H33	0.44	0.41	0.24	0.36
H34	0.27	0.38	0.04	0.29
H35	0.35	0.44	0.10	0.37

4. Conclusion

The present study successfully developed a compound 4-Nitroaniline Picric Acid with notable nonlinear optical (NLO) properties. High-quality single crystals were obtained through the slow evaporation technique. Powder XRD analysis confirms the crystalline nature of the compound. Functional groups present in the crystal was identified using FT-IR and FT-Raman spectroscopy. Thermal stability of the compound was confirmed by TG/DTA analysis and the title compound is stable up to 298°C. HOMO-LUMO energy gap of 3.257 eV indicates the intramolecular charge transfer between the molecules. The small energy gap allows easy electron excitation, creating excellent conditions for nonlinear optical performance. Natural bond orbital analysis showed significant charge transfer within the molecule, mainly from strong $n \rightarrow \pi^*$ interactions. This charge movement increases the molecule's polarizability, boosting nonlinear susceptibility. The findings highlight the material's strong potential for nonlinear optical applications.

References

[1] Mojca Jazbinsek, Uros Puc, Andreja Abina and Aleksander Zidansek, Appl. Sci., 9(5), 882 (2019); https://doi.org/10.3390/app9050882

[2] Yulin Huang, Wenfa Zhou, Xiaofang Li, Li Jiang, Yinglin Song, Materials Advances, 2, 2097-2103(2021); https://doi.org/10.1039/D0MA00918K

[3] R. Kaliammal, G. Parvathy, G. Maheshwaran, V.Kousalya Devi, M.Krishna Kumar, K. Sankar Anarayanan, S. Sudhahar, Journal of Molecular Structure, 1254, 132330 (2022); https://doi.org/10.1016/j.molstruc.2022.132330

[4] M. Shankar, K. Thirupugalmani, K. Nehru, S. Athimoolam, V. Tamilmani, I. Vetha Potheher, Journal of Molecular Structure, 1243, 1309055 (2021); https://doi.org/10.1016/j.molstruc.2021.130905

[5] Deepak Devadiga, Juchao Yan, Dheeraj Devadiga, ACS Appl. Energy Mater. 8, 4, 1942-1963 (2025); https://doi.org/10.1021/acsaem.4c03246

[6] N. Sudha, R. Surendran, S. Jeyaram, Optical Materials,131,112668(2022); https://doi.org/10.1016/j.optmat.2022.112668

[7] B. Babu, J. Chandrasekaran, R. Thirumurugan, K. Anitha, M. Saravanabhavan, Optics & Laser Technology, 94, 253-2601 (2017); https://doi.org/10.1016/j.optlastec.2017.04.007

[8] Rakhi Sreedharan, Sarath Ravi, K. R. Raghi, T. K. Manoj Kumar, K. Naseema, S N Applied Sciences,2,578(2020); https://doi.org/10.1007/s42452-020-2360-9

[9] Ye-Tao Chen, Ming-Peng Zhuo, Xinyi Wen, Wenbin Chen, Ke-Qin Zhang, Ming-De Li, Adv Sci (Weinh), 10(11),2206830(2023); https://doi.org/10.1002/advs.202206830

[10] M. Manonmani, C. Balakrishnan, S.Rafi Ahamed, G. Vinitha, S.P. Meenakshi Sundaram, R.M. Sockalingam, Journal of Molecular Structure,1190, 1- 10(2019); https://doi.org/10.1016/j.molstruc.2019.04.010

[11] J. Frisch, et al., Revision C.01, Gaussian, Inc., Wallingford CT. (2010)

[12] A.D. Becke, J. Chem. Phys. 98, 5648 (1993); https://doi.org/10.1063/1.464913

[13] G. Rauhut, P. Pulay, J. Phys. Chem. 99, 3093(1995); https://doi.org/10.1021/j100010a019

[14] A Ali, Y W Chiang, R M Santos, Minerals 2022. 12,205 (2022); https://doi.org/10.3390/min12020205

[15] C F Holder, R E Schaak, ACS Nano, 13,7359-7365(2019).

https://doi.org/10.1021/acsnano.9b05157

[16] Y Priya, K Rao, P Chalapathi, A Veeraiah, Journal of Modern Physics, 9, 753-774 (2018); https://doi.org/10.4236/jmp.2018.94049

[17] P K Sivakumar, M krishna Kumar, R Mohan Kumar, R Kanagadurai, Modern physics letters B. 32, 1350235 (2013); https://doi.org/10.1016/S0262-4079(13)62904-8

[18] K I Hadjiivanov, D A Panayotov, M Y Mihaylov, E Z Ivanova, K K Chakarova, S M Andonova,N L Drenchev, Chem. Rev. 121 ,1286-1424 (2020); https://doi.org/10.1021/acs.chemrev.0c00487

[19] Restiani Alia Pratiwi, Asep Bayu Dani Nandiyanto, Indonesian Journal of Educational Research and technology, 1, 1-20 (2022); https://doi.org/10.17509/ijert.v2i1.35171

[20] LRB Santos, T Chartier, C Pagnoux, JF Baumard, CV Santillii, SH Pulcinelli, A Larbot, Journal of the European Ceramic Society,24,15-16 (2004); https://doi.org/10.1016/j.jeurceramsoc.2004.03.003

[21] Shivani, Akriti Mishra, Paramjit Kaur, and Kamaljit Singh, ACS Omega. 7, 39045-39060 (2022); https://doi.org/10.1021/acsomega.2c04795

[22] B Mohanbabu, R Bharathikannan, G Siva G, Journal of Optoelectronics and Advanced Materials. 17, 1603-1614 (2015).

[23] E. Shobhana, B. Babu, B. Mohanbabu, V. Sathyanarayanamoorthi, Asian Journal of Chemistry. 11, 2603-2617 (2023); https://doi.org/10.14233/ajchem.2023.28258

[24] J. Hu, J. Wu, D. Jin, S.T. Chu, B.E. Little, D. Huang, R. Morandotti, D.J. Moss, Sensors 2023. 23, 9767 (2023); https://doi.org/10.3390/s23249767

[25] S. Krishna Priya, R. Karunathan, E. Shobhana, B. Babu, R. Kesavasamy, S. Akila, M. Karpagavalli, AIP Conf. Proc. 2446, 100008 (2022); https://doi.org/10.1063/5.0108265

[26] R Thayala Sanker, S Arunachalam, S Raju, M Velayutham Pillai, R Kumaresan, Int. Res. J. Multidiscip. Technovation, 6, 155-171 (2024); https://doi.org/10.54392/irjmt24112

[27] A Mohamed Ibrahim, S Arunachalam, J Suryakanth, M Velayutham Pillai, Int. Res. J. Multidiscip. Technovation, 5, 20-26 (2023); https://doi.org/10.54392/irjmt2343

[28] S Ahmad Siddiqui, M Margub Abdullah, Materials Today Communications. 22, 2352-4928 (2020); https://doi.org/10.1016/j.mtcomm.2019.100788

[29] S. Selvaraj, Int. Res. J. Multidiscip. Technovation, 6(1), 1-16 (2024); https://doi.org/10.54392/irjmt2411

[30] C. Helene, G. Lancelot, Prog. Biophys. molec. Biol. 39, 1-68(1982); https://doi.org/10.1016/0079-6107(83)90013-5

[31] A Ali, M Khalid, M F ur Rehman, S Haq, A Ali, M.N. Tahir, A.A.C Braga, ACS Omega. 5,15115-15128 (2020); https://doi.org/10.1021/acsomega.0c00975

[32] D.E. Moreno, C.Z. Hargather, Solids 2023. 4, 327-343 (2023); https://doi.org/10.3390/solids4040021